SECTION VII

Target Studies

Particle Accelerators, 1992, Vols. 37–38, pp. 495-504
Reprints available directly from the publisher
Photocopying permitted by license only

IMPLOSION SYMMETRY REQUIREMENTS FOR HIGH GAIN ICF

STEFANO ATZENI

Associazione EURATOM-ENEA sulla Fusione, Centro Ricerche Energia Frascati, C.P. 65, 00044 Frascati (Rome), Italy.

(Received 3 December 1990)

Some aspects of the problem of the implosion symmetry in Inertial Confinement Fusion (ICF) are discussed, with particular reference to heavy-ion-beam fusion. The physics of ignition of a target imploded by a driving pressure with long wavelength (low-l Legendre modes) asymmetries has been studied by means of 2-D simulations. A parametric study shows that the tolerable level of non-uniformity is a decreasing function of l, with the actual values depending on the specific target features (such as convergence ratio and ignition margin). The isobaric-fuel model of gain is then used to show how symmetry constraints (which limit the convergence ratio and the hohlraum transfer efficiency) affect the fuel energy gain. By using a model of ion beam energy conversion to X-rays, the gain of a class of indirectly driven targets is also estimated as a function of the relevant beam parameters.

1 INTRODUCTION

The problem of implosion symmetry is crucial for Inertial Confinement Fusion (ICF) research, since high gain requires high fuel compression and central, hot-spot-triggered ignition.[1–3] The allowed asymmetries of the compressed fuel are thus limited to scales smaller than the compressed fuel radius R_C, and of the hot spot radius R_H, respectively, both being a small fraction of the initial radius R_0.

In this paper we restrict our attention to long wavelength asymmetries (low-l Legendre modes, in 2-D) of the driving pressure, such as those associated to the finite number of beams (in direct-drive ICF), to the hohlraum geometry (in indirect-drive ICF), and to pointing and synchronization errors. We shall neglect short-scale target defects and irradiation non-uniformities, which seed the Rayleigh–Taylor instability. In doing this we assume that suitable measures (including use of moderate-aspect-ratio targets, with appropriate choice of the materials, pulse shaping, etc.) have been taken to minimize instability growth and the consequent mixing. In Section 2, we briefly summarize recent 2-D numerical work on the sensitivity of high gain targetsto to implosion asymmetries.[4] The effect of the symmetry constraints on the gain curves for ICF, and in particular, for heavy ion fusion (HIF), is discussed in Sections 3 and 4 by using a simple target model and a recently derived expression of ion beam to X-ray conversion efficiency[5–6].

2 LONG-WAVELENGTH IMPLOSION ASYMMETRIES AND BURN EFFICIENCY

The sensitivity of a target to implosion asymmetries, in general, depends on many details of the implosion history. However, we expect that if we restrict attention to a given family of targets, and to single-mode perturbations of the driving pressure, the burn degradation due to the asymmetry will depend on a small number of parameters. For instance, we may refer to gas-filled shells like that of Figure 1a, and to perturbations of the driving pressure characterized by the mode number l and the peak to valley amplitude $\Delta p/p$. In such a case the burn degradation should depend only on the product $C_H \Delta p/p$ (where $C_H = R_0/R_H$ is the hot spor convergence ratio) and the *ignition margin* (the margin between the actual, 1-D spot size and the spot size corresponding to the ignition threshold). This follows from the fact that, during the acceleration stage, secular deformations of the target occur, leading to the creation of a hot spot with relative deformation $\xi \simeq C_H \Delta p/p$. The subsequent interaction with reflected shocks, and the Rayleigh–Taylor instability of the hot-spot boundary, will often lead to further growth of ξ. The larger the deformation, and the higher l, the larger the energy losses from the hot spot and the slower the self-heating process. For deformations larger than some threshold, also depending on the ignition margin, ignition will not occur.

The above discussion is in agreement with a 2-D numerical study[4] performed with the code DUED (in its 2-T version, including α-particle diffusion and a rough model

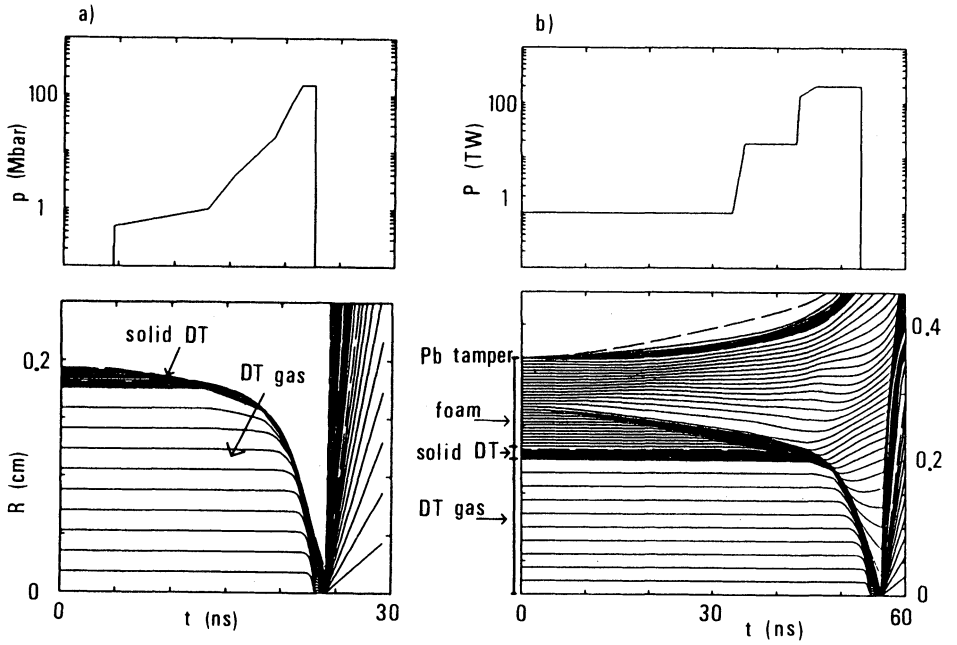

FIGURE 1 Part a, left: D-T shell considered in the study on implosion asymmetry. Upper frame: applied pressure vs time; lower: 1-D radius-vs.-time trajectories of Lagrangian mesh points. Part b, right: typical implosion driven by a heavy ion beam (4 GeV Bi ions); here the upper frame shows beam power vs. time.

for radiation losses). For simplicity, we have considered simple D-T shells (see Figure 1a), imploded by time-shaped pressure pulses rather than irradiated by a certain driver. The target structure and the pressure pulse were chosen to reproduce the implosion dynamics of a high-gain direct drive laser fusion target design[7], but some high-gain heavy ion target concepts[8] also have similar implosion characteristics (see Figure 1b, from a 1-D, 3-T simulation; this target is irradiated 2 MJ of 4 GeV Bi ions, and achieves a gain $G \simeq 100$).

The yield degradation for increasing mode amplitude for modes $l = 2, 4, 8$ is shown in Figure 2 for two cases, with approximately the same hot spot convergence ratio $C_H = 35$–40, but different ignition margins. The maximum tolerable asymmetry decreases with mode number; the trend is general, but the actual numerical values depend heavily on details of the target and of the pressure pulse. It turns out, however, that even in the best cases the peak-to-valley $\Delta p/p$ must be limited to about 4% for $l = 4$ and to 1.5% for $l = 8$. Also, for $l = 4$, the product $C_H \Delta p/p$ must in any case be smaller than about 2. (Caution is needed in appraising these figures because of the code's rough modeling of radiation; errors are also introduced, in the form of numerical diffusion, by the mesh re-zoning method, which in some cases makes the results dependent on details of the mesh; this is the origin of the large error bar represented by the shaded area in Figure 2b).

Ignition and burn in 2-D are illustrated in Figure 3. Here we see that during the self-heating stage, the hot-spot is being deformed by the Rayleigh–Taylor instability, whose growth halts when the burn wave eventually propagates. Figure 4 shows that if the stagnation is longer than in the previous case (which we have simply obtained by artificially switching-off the α-particle heating), the Rayleigh–Taylor spikes grow further, up to the point where the hot spot is destroyed. This indicates the need of tailoring the implosion in such a way that the interval between the onset of the instability and ignition be minimized.

With regard to heavy ion fusion, the need for very high uniformity for modes $l \geq 8$, together with concern for the Rayleigh–Taylor instability of the interface between

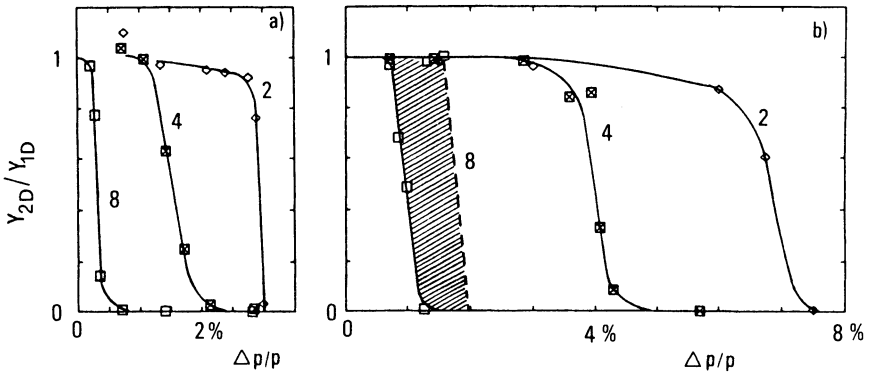

FIGURE 2 Yield (Y) degradation due to 2-D effects: $Y_{2\text{-D}}/Y_{1\text{-D}}$ vs. peak-to valley $\Delta p/p$ for modes $l = 2, 4,$ and 8, for two targets similar to that of Figure 1. Part a, left: a marginally igniting target. Part b, right: the best case considered. Curves are labeled by the value of l. For the meaning of the dashed area in Figure 2b see the main text.

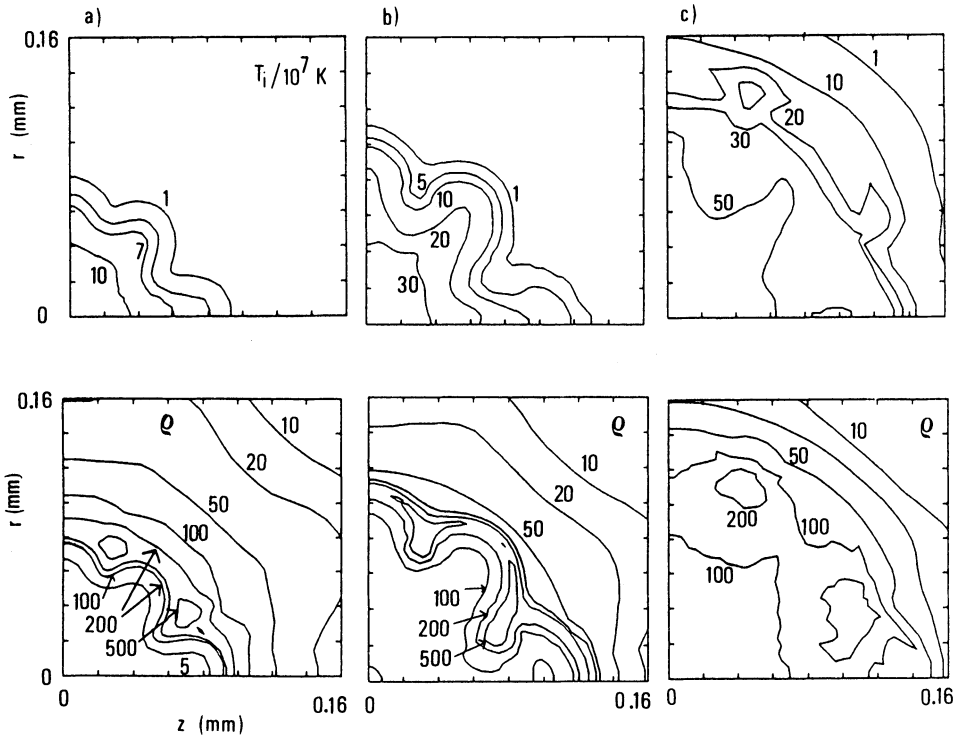

FIGURE 3 Ignition and burn of a target as in Figure 1a, imploded by a pressure pulse with $l = 8$ and peak-to-valley ratio $\Delta p/p = 0.007$. Iso-ion-temperature contours (upper frames, in units of 10^7 K) and isodensity contours (lower, in g/cm^3) are shown at selected times: (a) $t = 23.920$ ns; (b) $t = 24.050$ ns; (c) $t = 24.090$ ns.

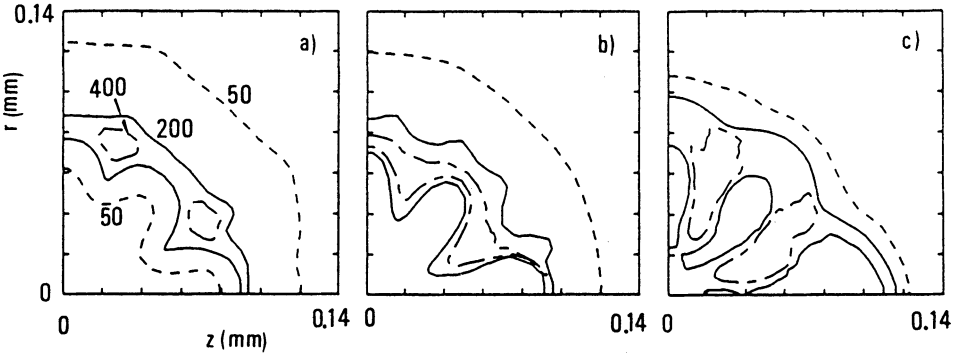

FIGURE 4 Rayleigh-Taylor instability at collapse, illustrated by a sequence of isodensity contours; (a) $t = 23.920$ ns; (b) $t = 24.000$ ns; (c) $t = 24.10$ ns.

fuel and pusher,[9] motivates the growing interest towards the indirect drive approach[10,11]. With such an approach, indeed, irradiation modes with $l \geq 8$ can be nearly suppressed[12–14] and Rayleigh-Taylor instability at the ablation front seems controllable[3].

3 SYMMETRY CONSTRAINTS AND TARGET GAIN

With the purpose of gaining insight into the effect of symmetry constraints on the target gain, we employ the isobaric model of fuel gain,[15] as improved by introducing a more adequate ignition criterion[16]. We consider a compressed D-T assembly, with mass M_{DT}, total energy E_{DT}, outer radius R_C, with a central hot spot of radius R_H, temperature T_H, and density ρ_H, such that the ignition criterion is satisfied (since the result depend very weakly on T_H[16], we use a fixed value of $T_H = 6$ keV). As usual[15,16] we write the specific energy and pressure of the cold fuel, with the latter equal to the hot-spot pressure, as α times (with $\alpha \geq 1$) those of a degenerate electron gas at the same density ρ_C, α being the so-called isentrope parameter. The fuel gain G_F is then computed as $G_F = Q_{DT}M_{DT}\phi/E_{DT}$, where $Q_{DT} = 3.4 \times 10^{11}$ J/g, and ϕ is the fractional burn-up, approximated as $\phi = \rho R/(\rho R + 7)$, with $\rho R = \rho_H R_H + \rho_C(R_C - R_H)$. [For analytic estimates we use $\phi = 0.135\ (\rho R)^{\beta}$, with $\beta = 0.7$].

We also introduce the initial fuel aspect ratio $A = R_0/\Delta R_0$ such that $M_{DT} = 4\pi\rho_s R_0^3/A$, where R_0 and ΔR_0 are respectively the initial target radius and thickness, and ρ_s is the solid D-T density.

Once the fuel gain is known, the target gain can be computed as $G(E) = \eta G_F(E_{DT})$, where E is the driver energy, η is the global efficiency, and $E_{DT} = \eta E$. In the case of indirect drive heavy ion ICF, where schemes such as that of Figure 5 can be

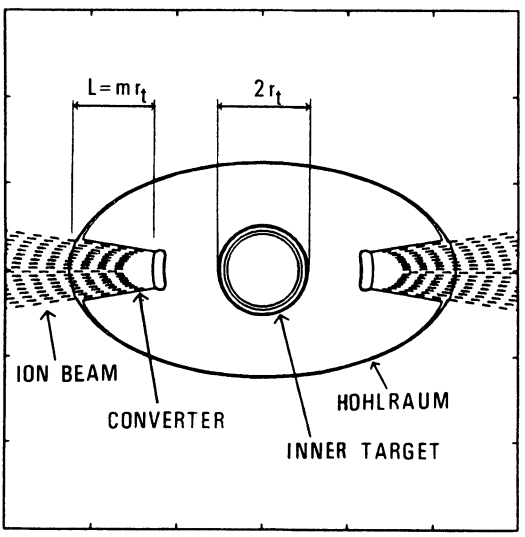

FIGURE 5 Schematic representation of an indirect drive target.

considered, one can write $\eta = \eta_X \eta_{tr} \eta_H$, where η_X is the X-ray conversion efficiency, η_{tr} is the transfer efficiency from the hohlraum to the inner capsule, and η_H is the hydrodynamic efficiency. For rough estimates one can take[14] $\eta_{tr} \simeq x$, for $0.2 \leq x \leq 0.6$, where x is the ratio of the target radius r_t to the typical linear dimension of the hohlraum. Larger values of x increase the efficiency,[13,14] but worsen the symmetry:[12-14] a reasonable trade-off value could then be $x = 0.3$.

Before discussing our results, it is worth recalling that while the above model is useful in showing trends, it cannot tell us much about the practical accessibility of a given compressed configuration. Also, we expect limited reliability of the model around the gain threshold.

We compute fuel gain curves $G_F(E_{DT})$ at constant fuel specific energy $\varepsilon = E_{DT}/M_{DT}$ (that is, at constant implosion velocity $v = (2\varepsilon)^{1/2}$), imposing a further constraint directly related to symmetry. We first consider the behavior of $G_F(E_{DT})$ at constant v and for constant values of C_H^3/A (here C_H is the hot spot convergence ratio defined above). Figure 6a refers to a case with $C_H^3/A = 4500$ (obtained by taking, for example, $C_H \simeq 35$, and $A = 10$). We observe that along each of the gain curves (solid curves in Figure 6a) α decreases with decreasing E_{DT}. The value $\alpha = 1$ thus sets a lower, optimistic threshold to each gain curve; more realistically, one has to consider larger values of α, which lead to higher threshold energies. It is also apparent that the higher v is, the lower the energy threshold for gain. For large E_{DT} we have

$$G_F \propto E_{DT}^{\beta/9} \varepsilon^{-1-(5/9)\beta} \left(\frac{C_H^3}{A}\right)^{2\beta/9},$$

which makes the beneficial effect of higher convergence apparent. This is also shown

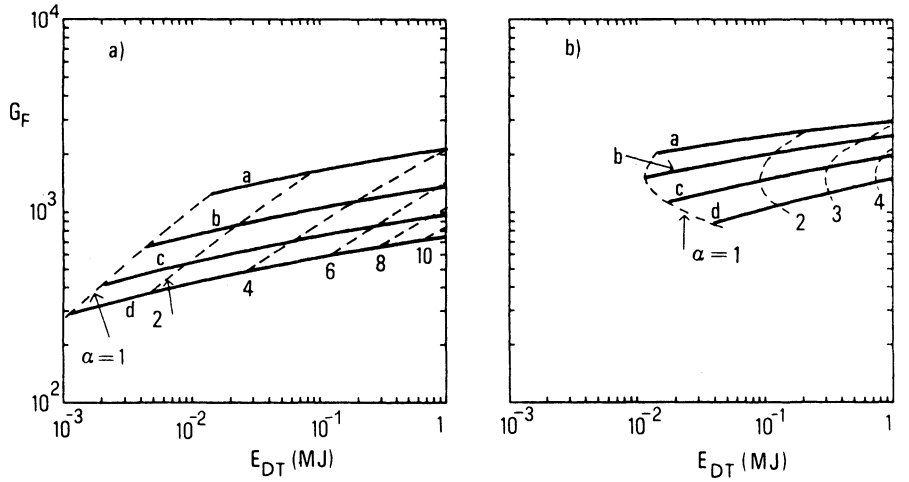

FIGURE 6 Part a, left: Fuel gain vs fuel energy for fixed $C_H^3/A = 4500$, and different implosion velocities v. (a) $v = 3.5 \times 10^7$ cm/s; (b) $v = 4.1 \times 10^7$ cm/s; (c) $v = 4.7 \times 10^7$ cm/s; (d) $v = 5.2 \times 10^7$ cm/s. Part b, right: same as Part a, but for $v = 3.5 \times 10^7$ cm/s and different values of C_H^3/A: (a) 3×10^4; (b) 10^4; (c) 3×10^3; (d) 10^3. Dashed lines join points of equal value of the isentrope parameter α.

by Figure 6b, where gain curves are shown for a given velocity and several values of C_H^3/A.

Analogous curves can be drawn by keeping constant the quantity C_c^3/A, where $C_C = R_0/R_C$ is the whole-fuel convergence ratio, which also means constant fuel pressure P for a given value of ε, since $P = 2\rho_S\varepsilon(C_c^3/A)$. In this case, for large E_{DT}

$$G_F \propto E_{DT}^{\beta/3}\varepsilon^{-1-(\beta/3)}\left(\frac{C_c^3}{A}\right)^{2\beta/3}.$$

Curves of the fuel gain $G_F(E_{DT})$ and of the target gain $G(E)$ are shown in Figure 7 for $C_c^3/A = 650$ and for three different values of v. Here we have required $\alpha \geq 2$ and then cut the gain curves with vertical lines at this threshold. We also show (with dashed vertical lines) the more conservative threshold obtained by requiring that $\rho_H R_H$ be 1.2 times larger than that prescribed by our standard ignition criterion. To draw the curves of $G(E)$ we have assumed $\eta_X\eta_{tr}\eta_H = 0.8 \times 0.3 \times 0.18$. We observe that the gain curves of Figure 7 show interesting analogies with those appeared in a recent LLNL paper[3].

4 X-RAY CONVERSION EFFICIENCY AND TARGET GAIN

For indirect drive heavy ion fusion, and with reference to the scheme of Figure 5, the previous results can be improved by evaluating explicity the X-ray conversion

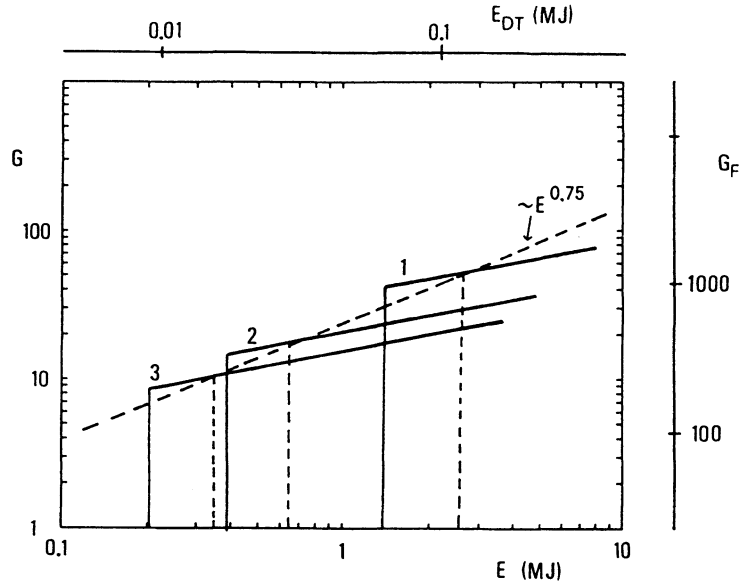

FIGURE 7 Thick solid lines: Fuel gain vs fuel energy and target gain vs driver energy for fixed values of $C_c^3/A = 650$ and $\eta = 0.0432$ (see main text), and for different values of the implosion velocity: (1) $v = 3.7 \times 10^7$ cm/s; (2) $v = 4.8 \times 10^7$ cm/s; (3) $v = 5.7 \times 10^7$ cm/s. For the vertical lines and the thick dashed line, see the main text.

efficiency as a function of the beam and target parameters. Recently,[5,6] it has been shown that, under certain restrictive assumptions and when backward losses are neglected, the conversion efficiency of a system of N identical cylindrical converters can be written as

$$\eta_x = 1 - K(Rr_0^{\delta})^{\delta_1} N^{\delta_2} \frac{1}{\hat{E}} \left[\frac{\hat{E}}{\hat{t} L^{1+\delta_4}} \right]^{\delta_3}, \tag{1}$$

where $K, \delta, \delta_1, \delta_2, \delta_3$, and δ_4 are constants depending on the converter material, $\hat{t} = t/(1\text{ ns})$, $\hat{E} = E/(1\text{ MJ})$, R is the ion range in cold matter, and r_0 and L are the converter radius and length, respectively. Of course, Eq. (1) is only meaningful when positive values of η_X are obtained. According to recent work[17], low density, high atomic number materials seem to be the best converters. We then consider converters made of low-density gold (e.g., supported by a foam structure). In this case $K = 280$, $\delta_1 = 1.32$, $\delta_2 = 0.68$, $\delta_3 = 0.32$, $\delta_4 = 1$ and $\delta = 1.52$ (in fact $\delta \simeq 1.5$ for many materials[5]).

We may at first consider how η_X scales for geometrically similar targets and hohlraums, with the targets being imploded at the same velocity and with the same hydrodynamic efficiency. In this case the term in square brackets in Eq. (1) is a constant, which is very close to unity for reasonable hohlraum-target configurations, so that we get

$$\eta_X \cong 1 - 450 \hat{E}^{-1} \left[Rr_0^{1.52} \left(\frac{N}{2} \right)^{0.52} \right]^{1.32},$$

which is plotted in Figure 8a, for $N = 2$ and for different values of $Rr_0^{1.52}$ We observe

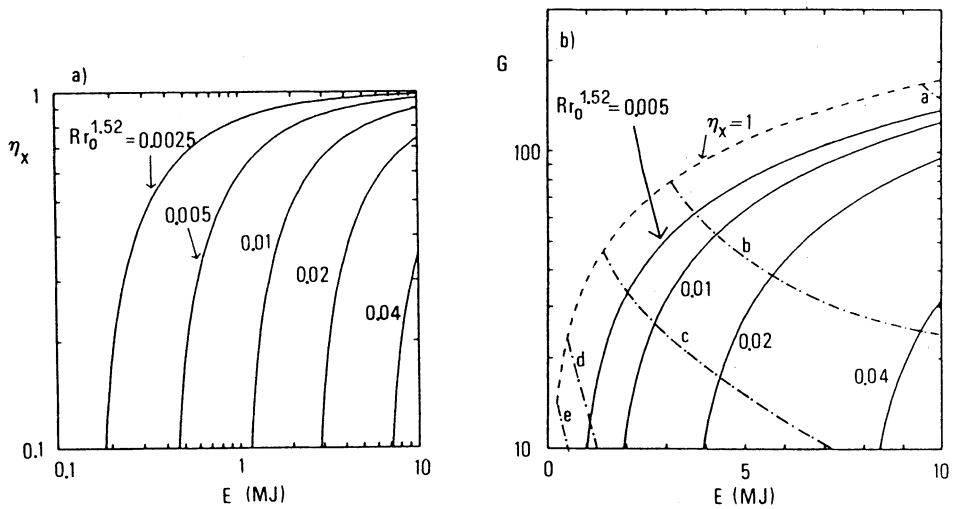

FIGURE 8 Indirect-drive heavy ion beam fusion. Part a, left: X-ray conversion efficiency η_X vs driver energy for a given family of targets, and for different values of the parameter $Rr_0^{1.52}$. Part b, right: Target gain vs driver energy for targets scaled as discussed in Sec. 4, for different values of $Rr_0^{1.52}$. The dot-dash curves are the loci of equal implosion velocity: (a) $v = 3 \times 10^7$ cm/s; (b) $v = 3.5 \times 10^7$ cm/s; (c) $v = 4 \times 10^7$ cm/s; (d) $v = 5 \times 10^7$ cm/s; (e) $v = 6 \times 10^7$ cm/s.

that for $R = 0.28$ g/cm^2 (10-GeV Bi ions on Au) and $r_0 = 0.1$ cm ($Rr_0^{1.52} = 0.0085$) we get $\eta_X \geq 0.8$ only for $E \geq 2.5$ MJ.

In conclusion, we apply Eq. (1) to a gain computation. We take the fuel gain given by the dashed, thick line of Figure 7 (the "envelope" of the "conservative" gain curves). Along such line $\varepsilon \propto M^{0.8}$, and the terms in square bracket in Eq. (1) have to be scaled accordingly. We now take roughly into account the backward radiation losses, by multiplying the value of η_X given by Eq. (1) by a factor of 0.9. We also assume $\eta_H = 0.18$ and $\eta_{tr} = 0.3$. The resulting gain curves for several values of $Rr_0^{1.52}$ are shown in Figure 8b. These curves closely resemble gain estimates published by LLNL scientists[10,11].

5 CONCLUSIONS

We have discussed the relationship between implosion symmetry and target gain. By means of implosion simulations we have shown how long-wavelength perturbations affect target gain, and have given orientative values of the allowed level of non-uniformity. By means of a simple gain model we have then shown how measures which reduce the sensitivity to non-uniformities (such as smaller convergence, or small ratio of capsule radius to hohlraum radius) severely constrain the gain. Also, we have shown that, in the case of indirect drive heavy ion fusion, the requirement of significant gain at modest energies (a few MJ) also sets stringent requirements on accelerator design and on the choice of the converter mass density.

The present study is, however, of a preliminary nature, with too many aspects of the problem needing further investigation before accurate, reliable predictions on gain curves and energy thresholds can be produced.

ACKNOWLEDGMENT

I thank Dr. J. Meyer-ter-Vehn and Dr. M. Murakami for several discussions on X-ray generation by ion beams, and for having made available to me prior to publication their results on radiation symmetrization physics.

REFERENCES

1. J. Nuckolls, L. Wood, A. Thiessen and G. Zimmerman, *Nature (London)* **239**, 139 (1972).
2. J. D. Lindl, in "Inertial Confinement Fusion," edited by A. Caruso and E. Sindoni, (Compositori-SIF, Bologna, 1989), pp 595 and 617.
3. E. Storm *et al.*, in *Proc. of the 13th International Conference on Plasma Physics and Controlled Nuclear Fusion Research*, Washington D.C., 1990 IAEA-CN-53/B-2-3 (IAEA, Vienna, in press).
4. S. Atzeni, *Europhys. Lett.* **11**, 639 (1990); *Laser Part. Beams*, **9**, 233 (1991).
5. S. Atzeni, "2-D Study of X-ray Generation from Ion Beam Heated Converters," these *Proceedings*.
6. S. Atzeni, J. Meyer-ter-Vehn and M. Murakami, to be published.
7. R. L. McCrory and C. P. Verdon, in Ref. 2, p. 183.
8. J. W.-K. Mark and J. D. Lindl, in *Heavy Ion Fusion* edited by M. Reiser *et al.*, (American Institute of Physics, New York, 1986), p. 441.
9. D. B. Kothe, J. U. Brackbill and C. K. Choi, *Phys. Fluids B* **2**, 1898 (1990).

10. R. O. Bangerter, *Fusion Technol.* **13**, 348 (1988).
11. J. D. Lindl, R. O. Bangerter, J. Mark, and Yu-LiPan, in Ref. 8, p. 89.
12. M. Murakami and K. Nishihara, *Jpn. J. Appl. Phys.* **25**, 242 (1986).
13. A. Caruso, in Ref. 2, p. 139.
14. J. Meyer-ter-Vehn and M. Murakami, "Analysis of Heavy Ion Fusion Targets," these *Proceedings*, and private communication.
15. J. Meyer-ter-Vehn, *Nuclear Fusion* **22**, 561 (1982).
16. S. Atzeni and A. Caruso, *Nuclear Fusion* **23**, 1092 (1983).
17. M. Murakami, J. Meyer-ter-Vehn and R. Ramis, *J. X-ray Sci. Technol.* **2**, 127 (1990).